Nanoscale

Accepted Manuscript

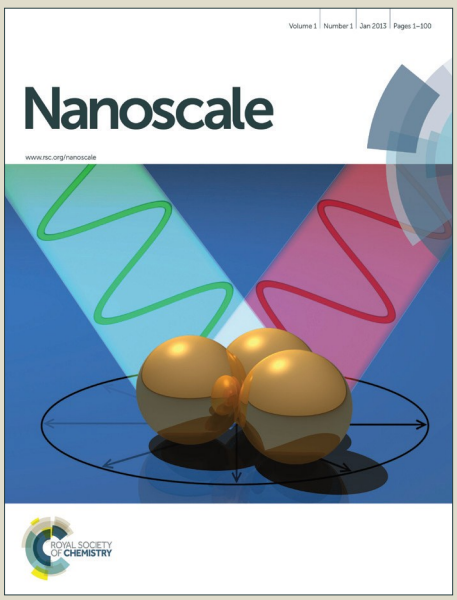

ROYAL SOCIETY OF CHEMISTRY

www.rsc.org/nanoscale

Journal Name

ARTICLE

Glyco-gold nanoparticle shapes enhance carbohydrate-protein interactions in mammalian cells.

Received 00th January 20xx,
Accepted 00th January 20xx

DOI: 10.1039/x0xx00000x

www.rsc.org/

Sivakoti Sangabathuni,[a] Raghavendra Vasudeva Murthy,[a] Preeti Madhukar Chaudhary,[a] Manalee Surve,[b] Anirban Banerjee[b] and Raghavendra Kikkeri[*a]

Advances in shape-dependent nanoparticles (NPs) research have prompted for a close scrutiny of the behaviour of nanostructures *in vitro* and *in vivo*. Data pertaining to the cellular uptake and the site specific sequestration of different shapes of NPs will undoubtedly assist to design better nano-probes for the therapeutic and imaging purposes. Herein, we investigated the shape dependent uptake of glyco-gold nanoparticles (G-AuNPs) in different cancer cell lines. Specifically, we have compared the behaviour of spheres, rods and star AuNPs with mannose and galactose conjugations. *In vitro* experiments showed that rod-AuNPs exhibited the highest uptake than that of the star and spherical counterparts. Further, investigation of the mechanism of uptake clearly demonstrated the clathrin mediated endocytosis of the specific G-AuNPs. These results reveal the benefits of different G-AuNPs shapes in carbohydrate-mediated interactions.

1. Introduction

Carbohydrates are the most abundant class of biomolecules on cell surfaces which are critically important for the cellular behaviour and functions and considered to be the first line of interaction between different pathogens, toxic materials, and between different cells.[1-2] Hence, carbohydrates are of central importance in the development of the next-generation biomarkers. However, the avidity of the monovalent carbohydrate-protein interactions is usually weak. Glyco-nanotechnology has provided multivalent scaffolds to increase the avidity of carbohydrate-mediated interactions and also has offered additional optical and electrochemical properties to develop biosensors and imaging tools.[3-5] In addition to the multivalency, the investigation showed that the size, orientation and density of the sugars on multivalent scaffolds can fine tune specific carbohydrate-protein interactions (CPI).[6-12] For example, Kiessling *et al.* have shown the importance of multivalent ligand architectures in CPI.[13] Penadés *et al.* developed a protocol to synthesize AuNPs with the hybrid-sugar system to explore its applications in blood brain barrier permeability, anti-HIV pro-drugs carrier.[14-16] Galan *et al.* developed glyco-quantum dots with defined glycan density and the nature of the oligosaccharide structures to tune the cell uptake and intracellular localization.[17] Seeberger *et al.* have shown the orientation and spatial arrangements of sugars that influence the relative activity.[18-19] Also, recent studies have demonstrated that the different shapes of the nanoparticles influenced the cellular uptake, biodistribution, and immune response.[20] High molecular stimulation *in vitro* and *in vivo* studies reported that elongated shapes have enhanced translocation rate over spherical ones and might have contributed to the structural evolution of pathogens such as bacteria and virus from spherical to rod-like morphologies. Among the existing shape dependent nanoparticles to date, gold nanoparticles have been at the forefront of nanotechnology research.[21-27] Questions regarding the shape dependent *in vitro* uptake and *in vivo* distribution have been thoroughly investigated by conjugating ligands such as antibodies, peptides, and aptamers to alter both the cytokine response, sequestration of NPs in different organs and clearance.[28-31] However, deciphering the shape dependent carbohydrate-mediated interactions undoubtedly assist in understand the origin of cell surface carbohydrates behaviour on endothelial, epithelial and neural cells which exhibit different shapes. To the best of our knowledge, no attempt has been made to study the shape-dependent CPI in *in vitro* models. Herein, we synthesized 3 different shapes of G-AuNPs and interpreted their roles in carbohydrate-mediated lectin binding and cellular uptake. Finally, we also studied the mechanism of cellular uptake of G-AuNPs using different pathway inhibitors. Our screening deciphers the role of shape in designing the next generation phenotypic specific drug delivery probes.

2. Results and discussion

Synthesis and lectin binding affinity of the G-AuNPs. PEG linker (1) and sugar ligands (2-3) (Fig. 1(i)) were covalently conjugated to AuNPs using previously reported ligand exchange processes.[32] To demonstrate the sensitive and selective binding between G-AuNPs and lectins, we performed ELISA plate inhibition assay using ConA, DC-SIGN and PNA lectins with G-AuNPs. Briefly, mannose-BSA and galactose-BSA, as reference ligands, were immobilized on a 96-well plate and treated with HRP-conjugated ConA or PNA lectins (1 mg/ml), in the presence of G-AuNPs, at different concentrations. In

[a]*Indian Institute of Science Education and Research, Pashan, Pune 411008, India. Fax: +91-20-25899790; Tel: +91-20-25908207; E-mail: rkikkeri@iiserpune.ac.in*
[b]*Indian Institute of Technology, Department of Bioscience and Bioengineering, Bombay-400076, India.*

† Electronic Supplementary Information (ESI) available: [details of any supplementary information available should be included here]. See DOI: 10.1039/x0xx00000x

case of DC-SIGN, lectin treatment was followed by HRP anti-IgG. After incubation, HRP was catalyzed and logarithmic curve for inhibition of lectin binding was plotted and IC_{50} values were determined. Table 1 summarizes the IC_{50} values of G-AuNPs. Mannose conjugated AuNPs exhibited substantial inhibition of ConA and DC-SIGN lectins, while galactose or PEG-conjugated G-AuNPs showed no affinity at all. Among three different shapes, rod-AuNPs exhibited nearly 3-fold more potent inhibition than spherical and star-shaped AuNPs. To demonstrate the possible selectivity of the binding, we performed inhibition assay with PNA lectin (Fig. S5). As expected, mannose-conjugated AuNPs didn't bind at all, while a significant inhibition was seen with galactose-coated AuNPs. Among the different shapes of AuNPs, rod-AuNPs once again demonstrated much more inhibition sensitivity compared to spherical and star counterparts. Overall, these results showed that the aspect ratio and surface to volume ratio of the rod-AuNPs influence the strong binding affinity with lectins.

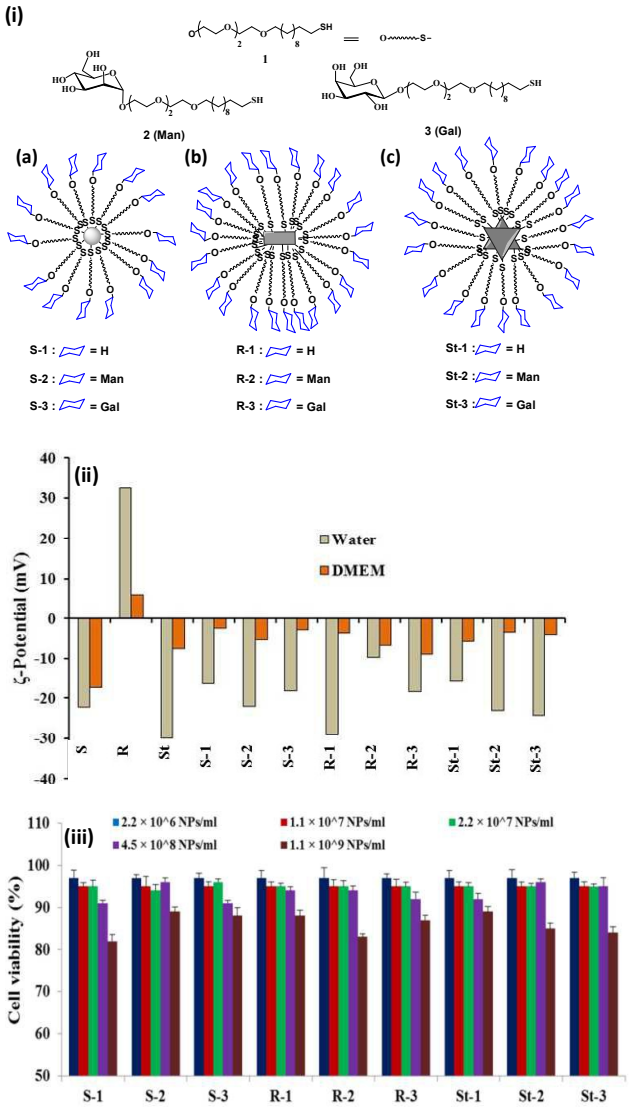

Fig. 1 (i) Structures of sugar conjugated AuNPs (G-AuNPs) (a) sphere; (b) rod and (c) star. (ii) Zeta potential of G-AuNPs in water and DMEM media. (iii) MTT assay showing the cell viability of sphere, rod and star shape G-AuNPs at 37 °C for 48 h incubation with HeLa cells.

Table 1. IC_{50} values of G-AuNPs for inhibition of lectins

G-AuNPs	ConA (Nps/ml)	DC-SIGN	PNA
S-2	2.6×10^6	4.3×10^6	-
R-2	9.5×10^5	1.1×10^6	-
St-2	1.4×10^6	2.7×10^6	-
S-3	-	-	2.5×10^6
R-3	-	-	8.7×10^5
St-3	-	-	1.3×10^6

Cellular cytotoxicity and uptake studies. The difference in the binding affinity of G-AuNps was further assessed in *in vitro* model. As the proteins present in the biological media can destabilize the NPs structures and functions, we first assessed the stability of the AuNPs in DMEM medium containing 10% FBS. The incubation of each AuNPs in biological medium showed no significant shift in the UV-visible profile after 24 h, which confirmed the stability of the shape and the size of the AuNPs. In contrast, the zeta-potential of the G-AuNPs varied quite significantly, indicating that the nanoparticles were surrounded by a soft layer of serum proteins and modulated the charge distribution on the GAuNPs (Fig 1(ii)). These results demonstrated that G-AuNPs retained their shape and stability in biological medium. All these results correlate to Chan *et al* results.[25]

After confirming the stability of the AuNPs, we investigated the uptake kinetics and mechanism using DC-SIGNtransfected and knockdown HeLa (human cervical cancer cells), HepG2 (hepatocellular liver carcinoma) and MDA-MB-231 (human breast cancer) cells.[33-39] To assess the relative toxicity of the GAuNPscell viability was evaluated using MTT assay in HeLa (cancer) and NIH-3T3 (normal) cell lines, incubated with different concentrations (2.2×10^6 – 1.1×10^9 NPs per ml) of PEGylated and G-AuNPs. It can be seen that both the HeLa and NIH-3T3 (Fig. 1(iii) & S4) cells did not show any significant cytotoxicity up to 4.5×10^8 NPs per ml even after 48 h. Hence, we set the above concentration as an ideal condition for further *in vitro* studies.

We then addressed the cellular internalization of G-AuNPs by measuring the gold concentration inside the cells. DC-SIGN-transfected HeLa cells were incubated with PEGylated and G-AuNPs for 4 h, 24 h, and 48 h respectively, followed by washing to remove unbound AuNPs. The cell pellets were dissolved in *aqua regia* solution and the gold concentration was quantified by inductively coupled plasma mass spectrometry (ICP-MS). The mannose-AuNPs exhibited the highest number of uptake compared to galactose or PEGylated-AuNPs in transfected HeLa cells. Among the different shapes of mannose-AuNPs, **R-2** showed approximately 3-fold increase in the number of NPs uptakes compared to **S-2** and **St-2** after 4 h incubation and this trend continued for next 24 h and 48 h (Fig. 2a-c). The probable reason for the highest number of rod-AuNPs uptake may be attributed to the fact that rod nanoparticles exhibited (1) aspect ratio, which could increase adhesion of particle to the cell surfaces, (2) high contact area of rod-AuNP with respect to external stimuli and (3) self-assembly of rod-AuPs. To confirm the selectivity, we also studied the nanoparticles uptake profile with DC-SIGN knockdown HeLa cells. ICP-MS clearly revealed the significant decrease in the mannose-AuNPs uptake, revealing the selective uptake of the AuNPs via receptors (Fig. 2d-f).[33-35] Further, we performed the uptake kinetics with MDA-MB-231, which has both mannose and galactose receptors.[36] ICP-MS results clearly revealed that the rod-AuNPs uptake is dominated compared to that

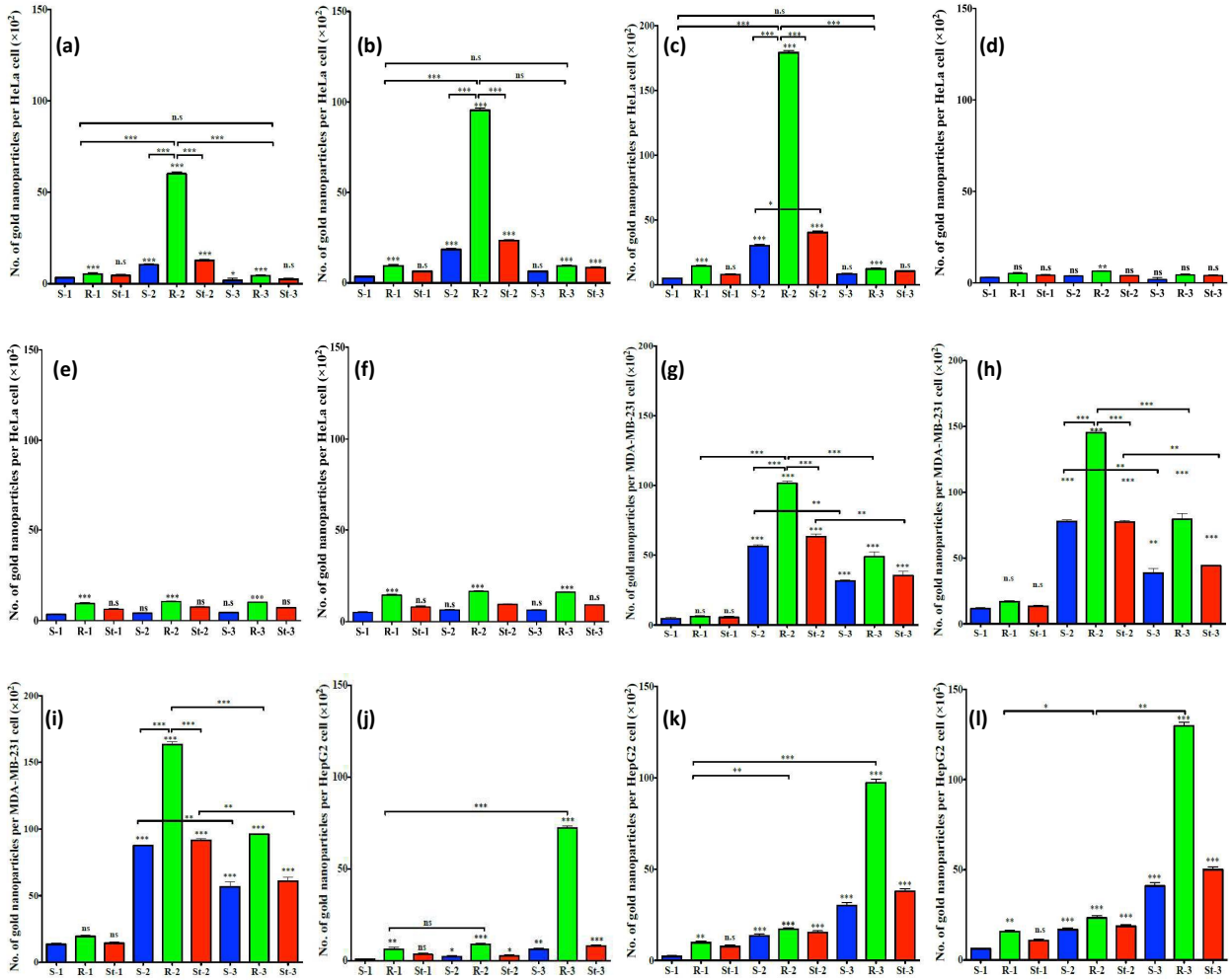

Fig. 2 Statistical analysis of ICP-MS data of HeLa (DC-SIGN transfected), HeLa (DC-SIGN knockdown), MDA-MB-231 and HepG2 at different time intervals. (a) HeLa-4h; (b) HeLa-24 h; (c) HeLa-48 h; DC-SIGN knockdown of (d) HeLa-4h; (e) HeLa-24 h; (f) HeLa-48 h (g) MDA-MB-231-4 h; (h) MDA-MB-231-24 h; (i) MDA-MB-231-48 h; (j) HepG2-4h; (k) HepG2-24h; (l) HepG2-48h. Data are presented as mean ±SEM for three independent experiments (***P<0.001, **P<0.01 *P<0.05 and n.s = not significant).

of two other shapes and we could see the uptake of both the mannose and the galactose-AuNPs (Fig. 2g-i). However, the number of mannose-AuNPs uptake was relatively higher than that of galactose-AuNPs, which indicated that the mannose receptors on the cell surfaces are more active than the galactose receptors. Finally, the above experiment was further confirmed with HepG2 cells, which has asialoglycan galactose receptors.[37-39] As expected, rod-AuNPs (**R-3**) was taken up much higher than other AuNPs **(**Fig. 2j-l). After 24 h and 48 h, the concentration of these AuNPs decreased. These results strongly suggest that nano-rods can induce specific fast uptake via carbohydrate receptors on the cell surfaces.

To validate the results with different cell lines with G-AuNPs, a more conventional dark field microscopic (DFM) imaging study was performed.[40] Figure 3i displays DFM images of DC-SIGN transfected HeLa, knockdown HeLa, MDA-MB-231 and HepG2 cells after 24 h incubation. In transfected HeLa cells, the bright spots from mannose-AuNPs (**S-2, R-2, St-2**) were observed close to the cell surfaces and in the cytoplasmic regions and the relative intensity of these bright spots was higher than PEG and galactose counterparts. Similar results were observed with the cell line MDA-MB-231 and HepG2 with respect to the carbohydrate receptors. Finally, the transmission electron microscopic (TEM) images of transfected HeLa cells were collected to confirm AuNPs sequestration. TEM images displayed a significant number of **R-2** sequestration in the cytoplasmic region compared to **S-2** and **St-2** (Fig. 3q-s). Moreover, we observed that the nano-rods were aligned parallelly and/or perpendicularly to each other. Overall, these results clearly showed that the shapes of the AuNPs indeed modulate the CPI.

Cellular Internalization pathway of R-2 in HeLa cells. To prove the mechanism of endocytosis, we utilized different known inhibitors for dynamin, clathrin and caveolae pathways to analyze the mechanism of internalization in DC-SIGN transfected HeLa cells.[41-42] Both ICP-MS and dark field imaging tools were used to analyze the data (Fig 3ii & 3iii). To evaluate the energy-dependent endocytosis, we incubated the cells with NaN_3 for 30 mins to deplete ATP, followed by the addition of **R-2** NPs for 4 h. We observed a strong decrease in cellular uptake of **R-2**, confirming the active endocytic pathway of internalization in HeLa cells. We

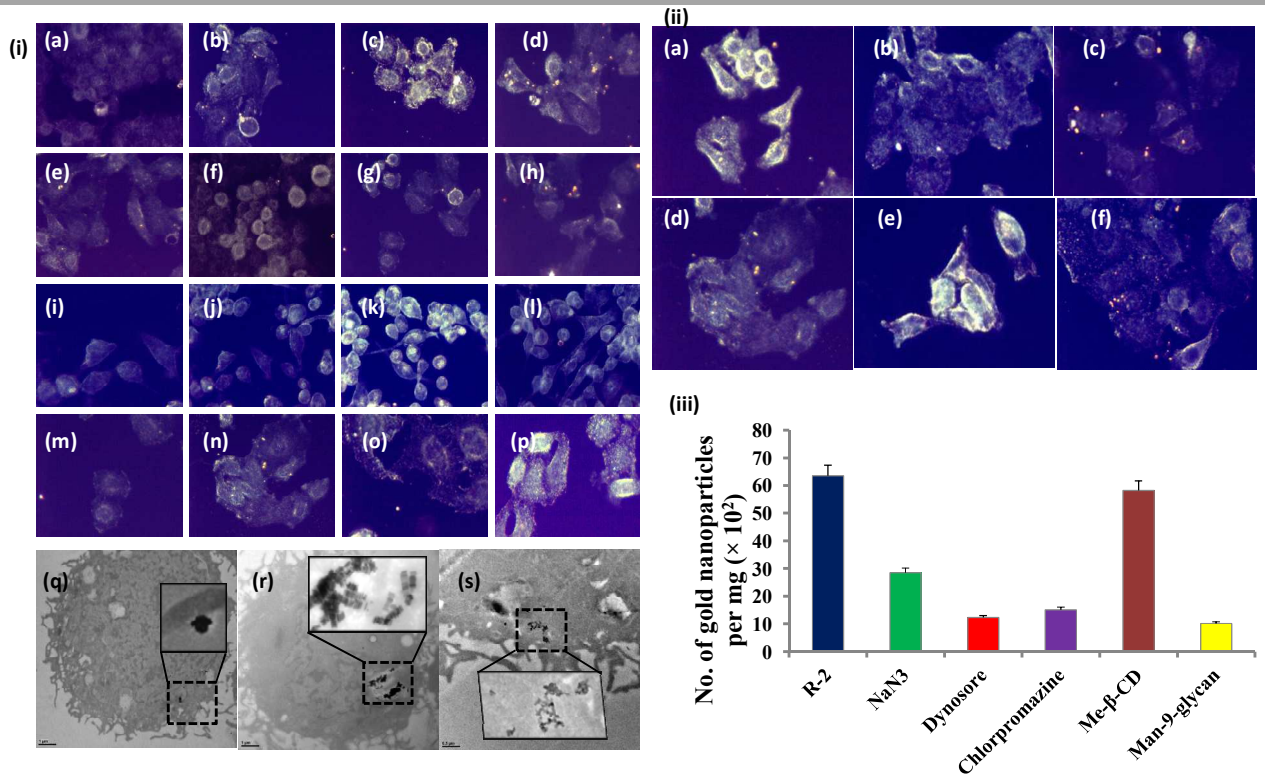

Fig. 3 (i) Dark field microscopic images of rod shape nanoparticles incubated with HeLa (DC-SIGN transfected), HeLa (DC-SIGN knockdown), MDA-MB-231 and HepG2 cells for 24 h at 37 °C. (a) HeLa-control; (b) HeLa, R-1; (c) HeLa, R-2; (d) HeLa, R-3; DC-SIGN knockdown of (e) HeLa-control; (f) HeLa, R-1; (g) HeLa, R-2; (h) HeLa, R-3; (i) MDA-MB-231-control; (j) MDA-MB-231, R-1; (k) MDA-MB-231, R-2; (l) MDA-MB-231, R-3; (m) HepG2-control; (n) HepG2, R-1; (o) HepG2, R-2; (p) HepG2, R-3. TEM images of HeLa cells contain (q) S-2; (r) R-2; (s) St-2 after 24 h. (ii) Dark field microscopic images of HeLa cells treated with inhibitor for 30 mins followed by **R-2** after 4 h. (a) control **R-2** after 4 h; (b) NaN_3 (50 mM); (c) dynosore (50 µM); (d) chlorpromazine (25 µM); (e) Me-β-cyclodextrin (10 mM); (f) Mannose-9-glycan (50 mM). (iii) Statistical analysis of ICP-MS data in presence and absence of inhibitor after 4 h. Data are presented as mean ±SEM for three independent experiments.

next established dynamin-dependent uptake. The addition of dynasore hydrate resulted in blocking dynamin function inhibiting the internalization of **R-2**, indicating that the internalization follows the conventional trend of clathrin or caveolae pathway. Further, we studied the effect of methyl-β-cyclodextrin (Me-β-CD), which inhibit caveolae-mediate endocytosis and chlorpromazine (inhibitor for clathrin-mediated endocytosis). As shown in figure 4, cells that were pre-treated with clathrin inhibitor showed a significant reduction in internalization, whereas, Me-β-CD pre-treatment showed negligible inhibition effect. These results validated that the **R-2** internalize *via* energy-dependent, clathrin-mediated endocytosis. Finally, we studied the uptake of **R-2** in the presence of Man-9-glycan that blocks the DC-SIGN receptor. The high mannose pre-treatment of cells dramatically reduce uptake of **R-2**. Altogether this clearly proves that **R-2** uptake depends on the DC-SIGN receptor on clathrin-mediated endocytosis. A similar experiment with HepG2 cells also revealed the clathrin-mediated endocytosis (Fig. S6).

3. Conclusions

A library of different shapes of glyco-AuNPs was synthesized and we used them as a tool to characterize the cellular uptake. ELISA plate lectin inhibition assay revealed that selectivity and sensitivity of the binding depended not only on the sugar composition but also was influenced by the shape of the AuNPs. *In vitro* experiments further supported the high affinity of rod-AuNPs compared to spherical and star counterparts. The mechanistic insight clearly demonstrated the clathrin-mediated mannose-dependent endocytosis. We anticipate that this shape-dependent enhancement of cellular uptake offers a new dimension to synthesize multivalent glyco-probes for diagnostic and therapeutic applications.[43-44]

4. Experimental Section

MTT assay

The cell viability was assessed by MTT (3-(4, 5-dimethylthiazol-2-yl)-2,5-diphenyltetrazolium bromide) assay in HeLa and NIH-3T3 cells. The NIH-3T3 and HeLa cells in monolayers were cultured in DMEM with 10% FBS medium in 100 mm cell culture dishes. Cells were trypsinized and plated at a density of 10,000 cells per well in a 96 well plate and once the cells got adhered, they were treated with varying concentration of AuNPs (number of nanoparticles) and incubated for 48 h. The medium was replaced and 10 µl of MTT was added to each well and incubated for 4 h at 37°C. Formazan crystals were dissolved in 100 µl of DMSO and absorbance at 570 nm was recorded using microplate reader.

Preparation of Cell samples for ICP-MS analysis

For the quantitative analysis of gold (Au) contents in the cellular uptake study, HeLa, MDA-MB-231 and NIH-3T3 cells (10^4 cells per plate) were incubated with the rod, sphere and

star AuNPs (5×10^8 nanoparticles) for 4h, 24h and 48h at 37 ºC. The medium was removed and cells were washed with PBS (3 times) before trypsinizing, centrifuged and the cell pellets were digested at 85 °C with 200 µl of fresh *aqua regia* for 4 h. Then each digested sample was diluted to 6 ml with Millipore water. The concentration of gold, determined by ICP-MS (Thermo-Fisher Scientific, Germany), was converted into the number of AuNP per cell.

Dark filed images of cell lines

Cellular uptake of AuNPs was examined using dark field microscopic images. HeLa, MDA-MB-231 and NIH-3T3 cells (10^4 cells per plate) were seed into 6 well plate with cover slip at the bottom and allowed to grow for 24 h in DMEM medium containing 10% FBS. Then cells were treated with AuNPs (5×10^8 nanoparticles) and incubated at 37 °C for 24h. Later, cells were washed 3 times with PBS and fixed with 4% paraformaldehyde at 37 °C for 15 min. The coverslips were then placed on the slide and fixed it with mounting media and dark field images were collected by exciting the cells with white light.

TEM images of cells containing nanoparticles

The uptake of different shapes of AuNPs by HeLa cells was assessed by transmission electron microscopy. HeLa cells (10^4) were seeded in 6-well plates at 37 °C for 4 h. Cells were treated with different shapes of AuNPs (5×10^8 nanoparticles) for 24 h at 37 ºC, followed by trypsinization. The pellet was fixed with 2.5% of glutaraldehyde in PBS for 4 h. The fixed cells were washed with PBS, further treated with 1% osmium tetroxide in water, then again washed with Millipore water for 2 times. The pellet was stained with 2% uranyl acetate in water for 1 h in dark after that the cells were again washed with water further dehydrated in ethanol (50%, 75%, 95% and 100%). The cell pellet was made into blocks by using Epon resin kit (DER 332, DER 732) by heating at 60 °C for 48 h. Sections of 70–90 nm thickness were cut on an ultramicrotome (RMC MTX) using a diamond knife. The sections were deposited on carbon-film copper grids and lead citrate treatment at room temperature for 3 min prior to TEM.

Cellular uptake mechanism

For all these experiments, DC-SIGN transfected HeLa cells were grown in 8-well chamber cover glass (1×10^4 cells/well) and treated with the specific inhibitor for 30 mins followed by **R-2** (5×10^8 NPs per ml) for 4 h at 37 °C. For energy dependent study, cells were incubated for 30 mins with NaN_3 (50 mM). For dynamin-mediated (clathrin and caveolae-mediated uptake) cells were treated with dynasore Hydrate (50 µM). For clathrin mediated uptake studies chlorpromazine (25 µM) were added. For caveolae mediated uptake, cells were treated with methylated-β-cyclodextrin (10 mM). For mannose-dependent uptake, cells were treated with high mannose glycans (1µg) for 30 mins. After 4 h of **R-2** treatment, cells were washed to remove unbound materials, ICP-MS and dark field images of these samples were done as reported in respective sections. Similarly, we performed same experiments for HepG2 by incubating with **R-3**.

Acknowledgements

‡ Financial support from the IISER, Pune, Max-Planck partner group and DST (Grant No. SB/S1/C-46/2014) is gratefully acknowledged. P.M.C acknowledgment CSIR-RA, S.S thanks CSIR-JRF for supporting their fellowships.

Note and References

1 M. Cohen and A. Varki, *Int. Rev. Cell Mol. Biol.,* 2014, **308**, 75-125.
2 C. R. Bertozzi and L. L. Kiessling, *Science,* 2001, **291**, 2357-2364.
3 N. C. Reichardt, M. Martín-Lomas and S. Penadés, *Chem. Soc. Rev.,* 2013, **42**, 4358-4376.
4 M. Marradi, F. Chiodo, I. García and S. Penadés, *Chem. Soc. Rev.,* 2013, **42,** 4728-4745.
5 B. Kang, T. Opatz, K. Landfester and F. R. Wurm, *Chem. Soc. Rev.,* 2015, **44,** 8301-8325.
6 R. J. Pieters, *Org. Biomol. Chem.,* 2009, **7,** 2013-2025.
7 T. R. Branson and W. B. Turnbull, *Chem. Soc. Rev*., 2013, **42,** 4613-4622.
8 S. Zhang, Q. Xiao, S. E. Sherman, A. Muncan, A. D. Ramos Vicente, Z. Wang, D. A. Hammer, D. Williams, Y. Chen, D. J. Pochan, S. Vértesy, S. André, M. L. Klein, H. J. Gabius and V. Percec, *J. Am. Chem. Soc*., 2015, **137,** 13334-13344.
9 E. M. Munoz, J. Correa, R. Riguera and E. Fernandez-Megia, *J. Am. Chem. Soc*., 2013, **135,** 5966-5969
10 B. D. Polizzotti and K. L. Kiick, *Biomacromolecules,* 2006, **7,** 483-490.
11 R. Roy and T. C. Shiao, *Chem. Soc. Rev*., 2015, **44,** 3924-3941.
12 C. Fasting, C. A. Schalley, M. Weber, O. Seitz, S. Hecht, B. Koksch, J. Dernedde, C. Graf, E. W. Knapp and R. Haag, *Angew. Chem. Int. Ed*., 2012, **51,** 10472-10498.
13 J. E. Gestwicki, C. W. Cairo, L. E. Strong, K. A. Oetjen and L. L. Kiessling, *J. Am. Chem. Soc.,* 2002, **124,** 14922-14933.
14 F. Chiodo, M. Marradi, J. Park, A. F. Ram, S. Penadés, I. van Die and B. Tefsen, *ACS Chem. Biol.,* 2014, **9,** 383-389.
15 I. García, A. Sánchez-Iqlesias, M. Henriksen-Lacey, M. Grzelczak, S. Penadés and L. M. Liz-marzán, *J. Am. Chem. Soc.,* 2015, **137,** 3686-3692.
16 F. Chiodo, M. Marradi, B. Tefsen, H. Snippe, I. Van Die and S. Penadés, *PLoS. One,* 2013, **8,** e73027.
17 D. Benito-Alifonso, S. Tremel, B. Hou, H. Lockyear, J. Mantell, D. J. Fermin, P. Verkade, M. Berry and M. C. Galan, *Angew. Chem. Int. Ed.,* 2014, **53,** 810-814.
18 D. Grünstein, M. Maglinao, R. Kikkeri, M. Collot, K. Barylyuk, B. Lepenies, F. Kamena, R. Zenobi and P. H. Seeberger, *J. Am. Chem. Soc.,* 2011, **133,** 13957-13966.
19 D. Ponader, P. Maffre, J. Aretz, D. Pussak, N. M. Ninnemann, S. Schmidt, P. H. Seeberger, C. Rademacher, G. U. Nienhaus and L. Hartmann, *J. Am. Chem. Soc.,* 2014, **136**, 2008-2016.
20 L. A. Dykman and N. G. Khlebtsov, *Chem. Rev.,* 2014, **114,** 1258-1288.
21 F. Tian, M. J. Clift, A. Casey, P. Del Pino, B. Pelaz, J. Conde, H. J. Byrne, B. Rothen-Rutishauser, G. Estrada, J. M. de la Fuente and T. Stoeger, *Nanomedicine*, 2015, **10,** 2643-2657.
22 S. H. Cha, J. Hong, M. McGuffie, B. Yeom, J. S. VanEpps and N. A. Kotov, *ACS Nano*., 2015, **9,** 9097-9105.
23 K. C. Black, Y. Wang, H. P. Luehmann, X. Cai, W. Xing, B. Pang, Y. Zhao, C. S. Cutler, L. V. Wang, Y. Liu and Y. Xia, *ACS Nano*., 2014, **8,** 4385-4394.
24 H. Herd, N. Daum, A. T. Jones, H. Huwer, H. Ghandehari and C. M. Lehr, *ACS Nano*., 2013, **7,** 1961-1973.
25 B. D. Chithrani, A. A. Ghazani and W. C. Chan, *Nano Letters*., 2006, **6,** 662-668.
26 B. D. Chithrani and W. C. Chan, *Nano Letters*., 2007, **7,** 1542-1550.
27 S. Nangia and R. Sureshkumar, *Langmuir*, 2012, **28,** 17666-17671.

28 N. M. Schaeublin, L. K. Braydich-Stolle, E. I. Maurer, K. Park, R. I. MacCuspie, A. R. Afrooz, R. A. Vaia, N. B. Saleh and S. M. Hussain, *Langmuir*, 2012, **28,** 3248-3258.
29 J. Wang, G. Zhu, M. You, E. Song, M. I. Shukoor, K. Zhang, M. B. Altman, Y. Chen, Z. Zhu, C. Z. Huang and W. Tan, *ACS Nano,* 2012, **6,** 5070-5077.
30 X. Yang, X. Liu, Z. Liu, F. Pu, J. Ren and X. Qu. *Adv. Mater*., 2012, **24,** 2890-2895.
31 K. Niikura, T. Matsunaga, T. Suzuki, S. Kobayashi, H. Yamaguchi, Y. Orba, A. Kawaguchi, H. Hasegawa, K. Kajino, T. Ninomiya, K. Ijiro and H. Sawa, *ACSNano,* 2013, **7***,* 3926-3938.
32 P. M. Chaudhary, S. Sangabathuni, R. V. Murthy, A. Paul, H. V. Thulasiram and R. Kikkeri, *Chem. Commun*., 2015, **51,** 15669-15672.
33 D. Brevet, M. Gary-Bobo, L. Raehm, S. Richeter, O. Hocine, K. Amro, B. Loock, P. Couleaud, C. Frochot, A. Morére, P. Maillard, M. Garcia and J. O. Durand, *Chem. Commun.,* 2009, **28,** 1475-1477.
34 L. Tailleux, O. Schwartz, J. L. Herrmann, E. Pivert, M. Jackson, A. Amara, L. Legres, D. Dreher, L. P. Nicod, J. C. Gluckman, P. H. Lagrange, B. Gicquel and O. Neyrolles, *J. Exp. Med.* 2003, **197**, 121-127.
35 N. Sol-Foulon, A. Moris, C. Nobile, C. Boccaccio, A. Engering, J. P. Abastado, J. M. Heard, Y. Van Kooyk and O. Schwartz, *Immunity*, 2002, **16**, 145-155.
36 Y. Ma, H. Chen, S. Su, T. Wang, C. Zhang, G. Fida, S. Cui, J. Zhao and Y. Gu, *J. Cancer,* 2015**, 6**, 658-670.
37 S. K. Mamidyala, S. Dutta, B. A. Chrunyk, C. Préville, H. Wang, J. M. Withka, A. McColl, T. A. Subashi, S. J. Hawrylik, M. C. Griffor, S. Kim, J. A. Pfefferkon, D. A. Price, E. Menhaji-Klotz, V. Mascitti and M. G. Finn, *J. Am. Chem. Soc*., 2012, **134,** 1978-1981.
38 R. Kikkeri, B. Lepenies, A. Adibekian, P. Laurnio and P. H. Seeberger, *J. Am. Chem. Soc*., 2009, **131,** 2110-2112.
39 G. J. Berndardes, R. Kikkeri, M. Maglinao, P. Laurnio, M. Collot, S. Y. Hong, B. Lepenies and P. H. Seeberger, *Org. Biomol. Chem*. 2010, **8**, 4987-4996.
40 C. M. Treu, O. Lupi, D. A. Bottino and E. Bouskela, *Arch. Dermatol. Res.,* 2011, **303,** 69-78.
41 D. Suresh, A. Zambre, N. Chanda, T. J. Hoffman, C. J. Smith, J. D. Robertson and R. Kannan, *Bioconjug. Chem*., 2014, **25**, 1565-1579.
42 S. Kumari, S. Mg and S. Mayor, *Cell Res*., 2010, **20**, 256-275.
43 V. Shanmugam and S. Selvakumar, C. S. Yeh, *Chem. Soc. Rev*., 2014, **43**, 6254-6287.
44 R. Cao-Milán and L. M. Liz-Marzán, *Expet Opin. Drug. Deliv*., 2014, **11**, 741-752.